Enhanced 3D fluorescence live cell imaging on nanoplasmonic substrate

Enhanced 3D fluorescence live cell imaging on nanoplasmonic substrate

Manas Ranjan Gartia[1,5]**, Austin Hsiao**[2,5]**, Mayandi Sivaguru**[3]**, Yi Chen**[4,5] **and G Logan Liu**[2,4,5]

[1] Department of Nuclear, Plasma and Radiological Engineering, University of Illinois, Urbana, IL 61801, USA
[2] Department of Bioengineering, University of Illinois, Urbana, IL 61801, USA
[3] Institute for Genomic Biology, University of Illinois, Urbana, IL 61801, USA
[4] Department of Electrical and Computer Engineering, University of Illinois, Urbana, IL 61801, USA
[5] Micro and Nanotechnology Laboratory, University of Illinois, Urbana, IL 61801, USA

E-mail: loganliu@illinois.edu

Abstract
We have created a randomly distributed nanocone substrate on silicon coated with silver for surface-plasmon-enhanced fluorescence detection and 3D cell imaging. Optical characterization of the nanocone substrate showed it can support several plasmonic modes (in the 300–800 nm wavelength range) that can be coupled to a fluorophore on the surface of the substrate, which gives rise to the enhanced fluorescence. Spectral analysis suggests that a nanocone substrate can create more excitons and shorter lifetime in the model fluorophore Rhodamine 6G (R6G) due to plasmon resonance energy transfer from the nanocone substrate to the nearby fluorophore. We observed three-dimensional fluorescence enhancement on our substrate shown from the confocal fluorescence imaging of chinese hamster ovary (CHO) cells grown on the substrate. The fluorescence intensity from the fluorophores bound on the cell membrane was amplified more than 100-fold as compared to that on a glass substrate. We believe that strong scattering within the nanostructured area coupled with random scattering inside the cell resulted in the observed three-dimensional enhancement in fluorescence with higher photostability on the substrate surface.

S Online supplementary data available from stacks.iop.org/Nano/22/365203/mmedia

(Some figures in this article are in colour only in the electronic version)

1. Introduction

Fluorescence cell imaging is one of the most powerful and ubiquitous methods in cell biology research due to its specificity and high sensitivity [1]. Besides the instrumentation, the limitations to the sensitivity of fluorescence cell imaging include the quantum yield and photostability of the fluorophore and the auto-fluorescence of the cells. Due to the dynamic behavior exhibited by live cells, it is always desirable to look into the cellular processes with a high spatial and temporal resolution, and preferably for an indefinite duration of time. In addition, due to the heterogeneous nature of cell biology, often it is required to conduct the experiment at lower magnification, but with sufficient contrast to observe the cellular perturbation. Lower magnification generally results in lower collection efficiency and hence such studies are limited by the weakness of the fluorescence signal. The collection efficiency can be offset by using high numerical aperture (NA) lenses. Although this will improve the resolution (according to the Rayleigh criterion, the diffraction-limited lateral resolution, $r_{lateral} = C\lambda/(n \sin \alpha) \approx 0.61\lambda/\text{NA}$, where $C = \text{constant} = 0.61$ (coherence), $n =$ refractive index of medium between object and lens, $\alpha =$ semi-angle and λ is the wavelength of incident light. The axial resolution, $r_{axial} \approx 2n\lambda/\text{NA}^2$), using higher NA lens will result in losing the depth of field ($d = n\lambda/\text{NA}^2 + n\,r/(M\text{NA})$), where M is the magnification) [2]. Increasing NA or magnification results in a decrease of the depth of field and hence one need

to continuously focus up and down to probe the whole layer of a thick specimen [3]. This is a hindrance to automated high-throughput screening processes.

Although the weak fluorescence of traditional dyes (due to their comparatively low extinction coefficient) and low photostability of the molecular fluorophore (mainly due to irreversible chemical reactions with oxygen free radicals, commonly known as photobleaching) can be circumvented by using a new class of semiconductor nanocrystal probes, commonly called quantum dots, the low biocompatibility and blinking of the emission signal of quantum dots restricts the application in live cell imaging. Traditionally glass-or polymer-based substrates are used for cellular imaging. Due to higher refractive index of the substrate as compared to air, most of the fluorescence of the fluorophore is emitted into the substrate. Therefore, in the experimental set-up where the excitation and collection are performed on the same side (e.g. in an epifluorescence microscope, scanning microarray devices), the collection efficiency of light is very low. In fact, one study showed that only 20% of the total emitted light is collectible on standard glass substrates [4]. In order to increase the collection efficiency and to increase the fluorescence signal, recently a new strategy has been deployed by using metal-coated slides for cell imaging [5]. On a metal-coated mirror slides the intensity of the fluorescence signal can be increased by more than fourfold as compared to glass slides. The fluorescence enhancement has been attributed to two mechanisms: (1) mirror effect [6] and (2) surface plasmon resonance [7–11]. The reflection of the excitation light on the mirror substrate induces an enhancement of the excitation field and also the emitted light is redirected by the mirror substrate, towards the objective lens, thus increasing the collection efficiency [3]. However, the flat surface morphology limits plasmonic coupling and fluorescence enhancement efficiency [12]. In fact, plasmons are not created when flat metal surfaces are illuminated with light as surface plasmons are induced only under special optical conditions (Otto configuration or Kretschmann configuration, where the thin metal film is required to be illuminated through a glass prism or high refractive index material and at a precise angle) [13].

One such configuration used for cell imaging is known as total internal reflection fluorescence microscopy (TIRFM) [14]. In TIRFM a laser beam passes through a high numerical aperture (NA) objective and undergoes total internal reflection when reflected from a high refractive index medium (e.g. glass) into a low refractive index medium (e.g. cell/water). The electromagnetic evanescent wave thus produced penetrates the cell membrane adjacent to the coverglass and excites fluorophores within an ultra-thin optical section of ∼100 nm, thereby reducing background noise from out-of-focus fluorescence. However, because of a partial loss of light confinement due to light scattering in the cell, excited fluorophores in the inner part of the cell may contribute to background noise and compromise sensitivity. In addition, the above system, requiring a large incident angle and complicated optical systems (prisms and glass with high refractive) for the SPR coupling, makes it unsuitable for

imaging under commercial fluorescence microscopes or array readers. Another approach of enhancing fluorescence signal is by coupling light to localized surface plasmons (LSPR) which rely on the coupling of fluorophores to random distributions of metallic nanoparticles [15]. However, in order to get considerable enhancement precise control over spatial position of the fluorophore relative to the nanoparticle is required which makes these methods unsuitable for applications in cell imaging applications. Surface plasmons can also be coupled by subwavelength metal-coated gratings using excitation light from the same side as the grating surface [16–18]. The advantages of grating-coupled SPR as compared to prism-coupled SPR includes small resonance angle, higher coupling efficiency and simple optical set-up [12].

We recently reported a highly ordered nanopillar array for uniform surface enhancement Raman scattering (SERS) applications [19]. As opposed to ordered array structures, which can only support a few plasmonic modes, random array structures can support as well as localize large numbers of plasmonic modes [20]. In the present study, we have created a randomly distributed nanocone substrate on silicon and coated it with silver for surface-plasmon-enhanced fluorescence detection and cell imaging. We observed three-dimensional fluorescence enhancement on our substrate shown from the confocal fluorescence imaging of Chinese Hamster Ovary (CHO) cells grown on the substrate. Interestingly, the fluorescence intensity was amplified more than 100-fold as compared to glass substrates and the position of maximum intensity was more than 10 μm further away from the sample surface. The details of the fabrication, imaging and data analysis are presented in the following sections.

2. Materials and methods

2.1. Nanocone plasmonic structure fabrication

The nanocone structures are fabricated by photolithography and a reactive ion etching process. In order to make high-aspect-ratio nanocone structures, an etching–passivation method is used. First, the native oxide layer is removed from the polycrystal silicon wafer using a wet etch process (10:1 buffered oxide etching for 1 min). Then the required micro-area arrays (dot arrays) into which nanocone structures are to be etched are patterned by photolithography. Secondly, the polysilicon substrate is etched by HBr and oxidized by O_2 simultaneously. A PlasmaTherm SLR-770 Inductively Coupled Plasma (ICP) Reactive Ion Etcher (RIE) was used for the etching process. The temperature was set to 40 °C, the throat pressure was 20 mTorr, the RF power was 200 W and the etching time was 6 min during the fabrication process. The HBr flow rate was 20 sccm whereas the O_2 flow rate was set to 8 sccm. During etching, initially a nanomask made of silicon oxybromide naturally forms and then HBr gas etches the unmasked polysilicon substrate. Since HBr has a high etching selectivity of polysilicon to oxide (200:1), high-aspect-ratio nanopillar structures are formed. Finally, a thin layer of silver (80 nm) is deposited on top of the nanocone structures using e-beam evaporation to impart the plasmonic property. For better adhesion of metal to the nanocone Si substrate, 5 nm

of Ti layer was deposited before deposition of an 80 nm Ag layer. Prior to cell seeding, the nanocone substrate is sterilized by immersion in 70% ethanol for 2 h, followed by N_2 gas drying.

2.2. Cell culture

Chinese Hamster Ovary (CHO) cells are maintained in Ham's F12 medium containing 5% fetal bovine serum (FBS), 1% antibiotic–antimycotic solution (10 units ml^{-1} penicillin G sodium, 10 μg ml^{-1} streptomycin sulfate, 25 μg ml^{-1} amphotericin B, 0.85% saline; Invitrogen, Carlsbad, CA) and 1% glutamine and grown in 100 mm glass culture plates at 37 °C in a humidified atmosphere of 5% CO_2. The cells exhibit normal morphology, express cell contact inhibition and grow as a monolayer without expression of neoplastic foci. CHO cells are transferred when the culture becomes confluent. The CHO cell used in the experiment is CHO AS52 clone 11–4–8 with a cell division time of 24 h and takes up to 72 h (three days) for the culture to be confluent. For the experiment, the cells are re-suspended to 1×10^6 cells per ml. For the confocal imaging, the cells are seeded on the nanopillar plasmonic structure and incubated at 37 °C in a humidified atmosphere of 5% CO_2 for at least 12 h to allow attachment.

2.3. Cell labeling protocol

FM 1-43 FX (Cat # F35355, Invitrogen) dye is used to stain the cell membrane. A working staining solution of 5μl ml^{-1} dye in ice-cold PBS solution is prepared. The ice-cold temperature is used as the dyes are quickly endocytosed. Finally, the nanocone substrate with the cells is washed with fresh PBS before immersing in the staining solution for about 1 min. The substrate is immediately taken for imaging after staining.

Fluo-4, AM (Invitrogen, Carlsbad, CA) dye is used to monitor the calcium (Ca^{2+}) level of the cell and as a label for the viable cell cytoplasm. A working staining solution of 5 μl ml^{-1} dye in fresh PBS solution is prepared. The substrate with cells on top of it is washed with fresh media and then immersed in the staining solution. The substrate with the cells is incubated with the staining solution for 15 min at 37 °C in a humidified atmosphere of 5% CO_2 before imaging.

The cell nucleus is stained with blue fluorescent Hoechst dyes (Invitrogen, Carlsbad, CA). The substrate with the cells is incubated in a 2 μl ml^{-1} staining solution for about 15 min at 37 °C and a humidified atmosphere of 5% CO_2 before imaging.

2.4. Confocal imaging

The cell imaging is performed using a Zeiss LSM 710 Confocal Microscope (Carl Zeiss, Wake Forest, NC). The microscope system consists of a Zeiss 710 confocal scanner, Axio Observer Z1 microscope and a Spectraphysics Mai-Tai Ti–Sapphire laser. Three visible excitation lines (405, 488 and 561 nm) are used for our experiment. The microscope is equipped with a QUASAR 34 channel spectral detector (two standard PMTs and a 32-channel PMT array) with spectral resolutions up to 3 nm. ZEN 2009 software is used for hardware control and spectral un-mixing. The laser power used for the experiment is about 0.2% of the total available power (25 mW).

2.5. SEM fixation protocol for cells and SEM imaging

Initially, the cell media is replaced by a fixative solution (EM grade 2.0% paraformaldehyde and 2.5% glutaraldehyde in 0.1 M Na–Cacodylate buffer, pH 7.4) and kept for 4 h in a 4 °C refrigerator. Then the cells are rinsed with buffer solution (0.1 M Na–Cacodylate buffer, pH 7.4) for 10 min on a shaker table. After the buffer rinse, gradual dehydration (37% ethanol, 10 min; 67% ethanol, 10 min; 95% ethanol, 10 min; 100% ethanol, 3 min × 10 min) is performed for the cells. Finally, all the ethanol in the sample is replaced by carbon dioxide by performing critical point drying (CPD) in a 100% ethanol environment. Prior to SEM imaging the sample was sputter-coated with 7 nm gold–palladium coating and the imaging is performed using the Philips XL30 ESEM-FEG in Hi-Vac mode.

3. Results and discussion

Figure 1(a) shows a schematic overview of the experimental set-up. In the experiment living cells are situated on top of a nanocone substrate, which is composed of dense nanocone structures covered by a thin layer of silver. The silver-coated nanocone structures can support both propagating surface plasmons and localized plasmons in the visible wavelength range. Additionally the silver-coated nanocone structures are capable of 'nanofocusing' or 'concentrating' optical energy, creating a high electromagnetic field [21] that can be coupled to a cell. Figure 1(b) shows schematically a cell on a glass substrate and a cell on a nanocone plasmonic substrate, respectively. A scanning electron micrograph of the tapered silicon nanocone structures before and after coating with an 80 nm thick silver layer is shown in figures 1(c) and (d), respectively. The cross-sectional SEM in figure 1(c) shows a non-periodic array of nanocones covering the substrate. The nanocones are around 300 nm tall and 180 nm wide at the base. The average spacing between two adjacent silicon nanocones without silver coating is about 100 nm and the spacing is reduced to sub-50 nm after silver coating. Figures 1(e) and (f) show the scanning electron microscope images of spherical and elongated CHO cells on the nanocone structures.

3.1. Optical characterization of the substrate

Figure 2(a) shows the reflectance measurement for silver-coated nanocone structures in the visible range with normal incident and unpolarized light using a Varian Cary-5G. For comparison, the reflectance from a smooth silver mirror surface and smooth silicon surface is also plotted in the same figure. The observed low reflectance (<10%) is due to the so-called 'black silicon' surface roughness, where multiple reflections lead to strong, broad-band absorption and low reflectivity. This confirmed that most of the light incident on the nanocone substrate would be absorbed instead of reflecting back due to the metal surface. The reflectance spectrum of the nanocone substrate with silver coating showed a sharp dip in the reflectivity at 317 nm (figure 2(b)), which corresponds to the bulk plasmon for silver [22]. Another dip in the reflectivity is visible at 615 nm as shown in figure 2(b).
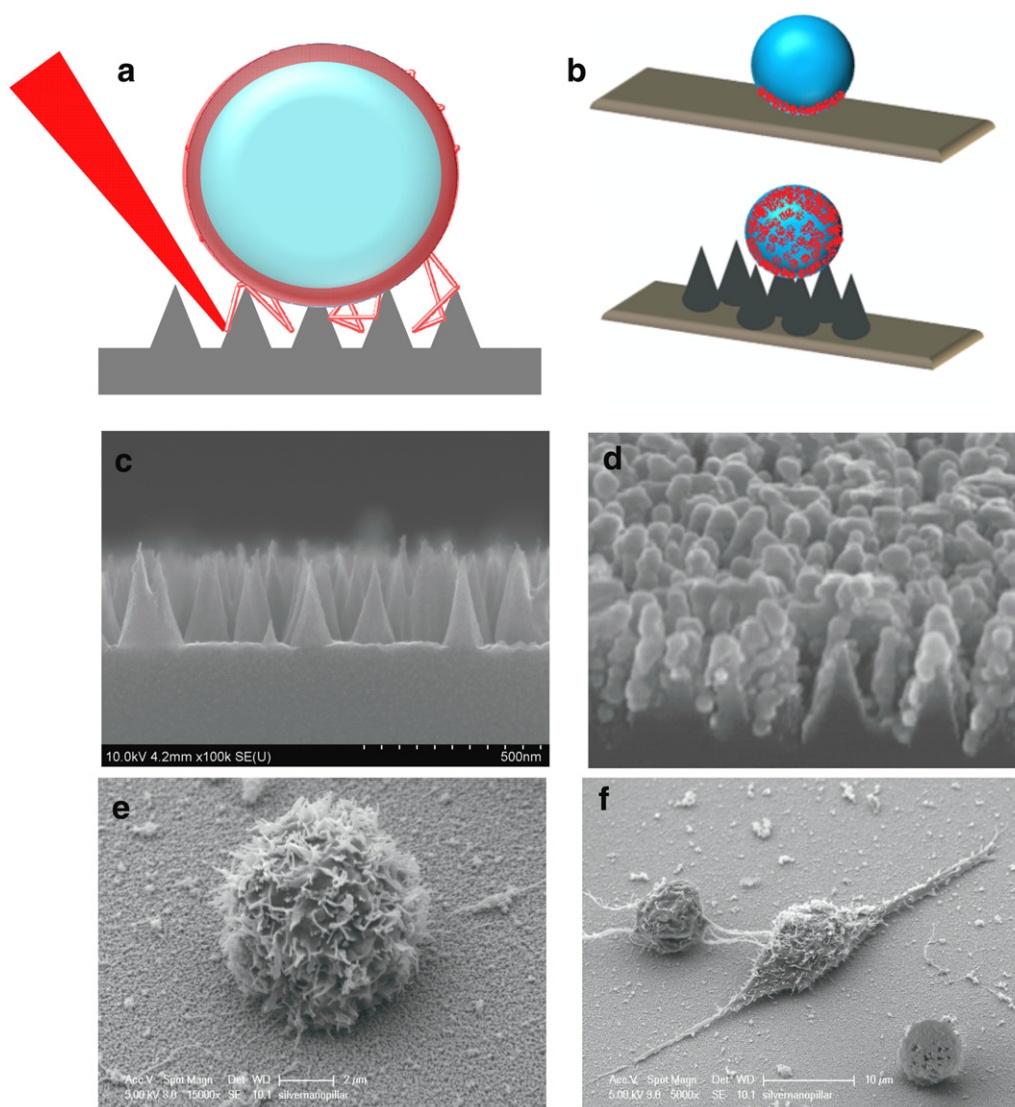
Figure 1. (a) Schematic illustration of coupling of light from the nanocone substrate into the cell for enhanced fluorescence. (b) Schematic illustration of enhancement observed when the cell is on a glass substrate and on a nanocone plasmonic substrate, respectively. (c) Scanning electron micrograph (SEM) of the fabricated silicon nanocone structure. (d) Nanocone structure after deposition of 80 nm silver and (e) SEM of a spheroidal CHO cell and an elongated CHO cell on the nanocone substrate.

Figure 2(c) shows the fluorescence spectroscopy data comparing the fluorescence intensity of R6G (5 μl of 10 μM solution dropped and allowed to dry) on a glass surface, silver-coated smooth silicon surface and silver-coated nanocone silicon surface, respectively. The intensity of fluorescence on a silver-coated smooth surface was about five times higher than that on a glass surface and the silver-coated nanocone surface showed fluorescence enhancement of about 40 times as compared to the glass surface. The enhancement of fluorescence efficiency on the nanocone structure may be due to plasmon resonance energy transfer from nanocone silver to the nearby R6G.

In order to confirm that our substrate can support surface plasmons we carried out a cathodoluminescence (CL) study. In traditional CL of semiconductors, the impingement of a high-energy electron beam results in the excitation of valence electrons to the conduction band, leaving behind a hole. The

detected photons in a CL spectroscopy experiment are a result of the recombination of electron–hole pairs. However, the detected photons in the case of a metallic nanostructure are a result of excited plasmons (collective motion of conduction electrons induced by fast moving electrons) [23]. The CL study for the nanocone structure showed that it can support a wide range of localized plasmonic modes and propagating surface modes. Figure 2(d) shows a CL spectrum collected from the nanocone structure and smooth silver surface from an area of 1200 nm × 800 nm. The spectrum is corrected for the grating response function. We observe a sharp peak at 331 nm and a small peak at 343 nm for the smooth silver surface. The sharp peak at 331 nm is generally attributed to the bulk plasmon peak and the peak at 343 nm is generally the surface plasmon peak [23]. For nanopillar plasmonic structures we observe a sharp peak with much higher intensity than that of the smooth surface at 363 nm, which corresponds to the
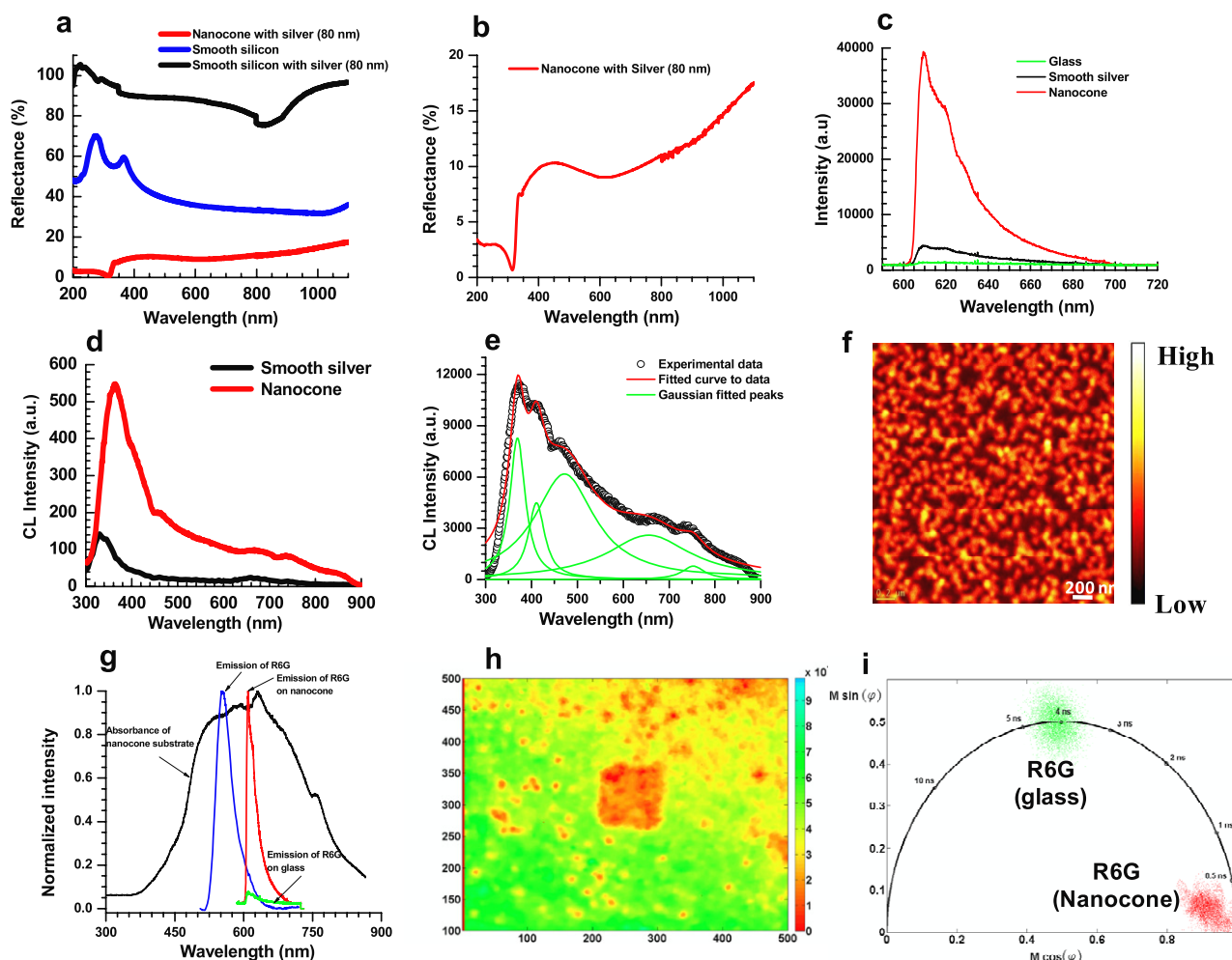
Figure 2. Optical characterizations of the substrate (a) reflectance measurement for smooth silicon, silver-coated smooth silicon and the silver-coated nanocone structure. (b) Reflectance measurement of nanocone structure showing the resonance (at particular wavelength). (c) Fluorescence intensity measurement on a fluorophore on a glass substrate, silver-coated smooth silicon and silver-coated nanocone structure using fluorescence spectroscopy. (d), (e) Cathodoluminescence (CL) spectrum collected from a nanocone structure. The spectrum is corrected for grating response function. (f) Panchromatic CL image (pseudo-colored) of the same area showing the intensity of surface and localized plasmon resonance. (g) Optical absorption spectra of nanocone substrate and emission spectra of Rhodamine 6G on a glass substrate and nanocone substrate. (h) Fluorescence lifetime imaging for Rhodamine 6G on a nanocone substrate. (i) Polar plot showing the lifetime quenching on the nanocone substrate for R6G.

surface plasmons at the silver–air interface [23]. In addition, light collected from a larger area (60 μm $\times$ 40 μm), after the deconvolution of the experimental data and the Gaussian fit revealed several surface plasmon peaks at 410, 472, 654 and 754 nm, indicating that our sample can support resonance for a broad range of wavelengths (figure 2(e)). Figure 2(f) describes the panchromatic CL image (pseudo-colored) of the same area showing the intensity of surface and localized plasmon resonance. The figure clearly showed many 'hot spots' for our nanocone substrate. The difference in the plasmon resonance mode observed in reflectance spectra and CL spectra may be due to the source of excitation for the plasmon. Light excitation can couple to low frequency plasmon eigenmodes, but may not excite all high frequency modes due to large momentum mismatch [17]. On the other hand, electron excitation can couple to high frequency modes [24]. Interestingly, the optical excitation of a model fluorophore (Rhodamine 6G) on

the nanocone surface showed an emission peak at 610 nm, which was the position of a reflectance dip observed in our earlier experiment (figure 2(b)). The dye R6G has an excitation wavelength and emission wavelength of 525 nm and 555 nm, respectively. For the optimum energy transfer to and from the fluorophore, a good spectral overlap between the emission band of the fluorophore and surface plasmon resonance band of the metallic substrate is required [25–27]. The absorption spectra of the nanocone substrate showed broad UV–vis absorption from 400–800 nm. Combined with the CL data, it can be inferred that the nanocone substrate has the surface plasmon band in between 1.55–3.1 eV (around 400–800 nm). The electronic transition energy of R6G from ground state to excited state is at 2.23 eV (around 555 nm), which allows the plasmon resonance energy transfer process between the dye molecule and the surface plasmon of the metal (figure 2(g)). The energy transfer process can happen in two

different ways. Surface plasmons of a nanocone substrate created due to excitation of light can transfer part of its energy to the fluorophore (R6G) (which is like an enhanced excitation mechanism for the fluorophore) and the fluorophore can then radiate, leading to an increase in fluorescence intensity. This is generally termed as mirror effect metal-enhanced fluorescence (MEF) or radiative decay engineering (RDE). The second mechanism relies on the strong coupling between the excited state of the fluorophore and plasmons. Here, the fluorophore in the excited state can interact with the metal nanostructure to create plasmons converting part of the fluorophore's non-radiative near-field emission to be radiated by surface plasmons as far-field emission (observed enhanced fluorescence). This is generally termed as surface plasmon coupled emission (SPCE) [28, 29]. Since there is a strong interaction between the surface plasmon and the excited state of the fluorophore, we are expected to see a modification in fluorophore properties such as lifetime and quantum yield on nanostructured surfaces. In fact, from our fluorescence lifetime imaging microscopy (FLIM), shown in figures 2(h) and (i), we observed a reduction in the lifetime of R6G on a nanocone plasmonic substrate. As the transfer of energy to the plasmon occurs on a shorter timescale and the plasmon radiates the emission quickly as well as efficiently, a reduction in fluorophore lifetime is expected [30]. For a typical comparison, the lifetime of R6G is about 4 ns whereas the photoexcited electron transfers from a metal substrate (gold) to adsorbed molecules in 200 fs [31]. The lifetime of a fluorophore in free space is given by $\tau_0 = 1/(\Gamma + k_{NR})$, where Γ is the radiative decay rate and k_{NR} is the non-radiative decay rate. Similarly, the quantum yield of a dye in free space can be written as $Q_0 = \Gamma/(\Gamma + k_{NR})$. Therefore, by measuring the lifetime and quantum yield, we can calculate both the radiative and non-radiative components of the fluorescence decay process as $\Gamma = Q_0/\tau_0$ and $k_{NR} = (1/\tau_0) - \Gamma$. Further, in the presence of a metal nanostructure, the quantum yield (Q_m) and lifetime (τ_m) of the fluorophore gets modified as $Q_m = (\Gamma + \Gamma_m)/(\Gamma + \Gamma_m + k_{NR,m})$ and $\tau_m = 1/(\Gamma + \Gamma_m + k_{NR,m})$, respectively [32]. It is interesting to note that, for fluorophores in free space, the quantum yield and fluorescence lifetime nearly always change in unison, whereas in the presence of metal surfaces as Γ_m increases, the quantum yield increases but the lifetime decreases. For example, from the quantum yield and lifetime measurement of R6G dye, the radiative decay rate and the non-radiative decay rate were 2.31×10^8 s^{-1} and 1.22×10^7 s^{-1}, respectively. In the presence of metal, the lifetime was reduced and the radiative decay rate was increased to 4.0×10^9 s^{-1} while the non-radiative decay rate was reduced to 8.0×10^6 s^{-1}. Further, the nanocone substrate showed good surface-enhanced Raman scattering (SERS) property (supplementary figure 1, available at stacks.iop.org/Nano/22/365203/mmedia). The details of the experiments are described elsewhere [19]. This showed that the nanocone substrate efficiently scatters light in the near-field and supports a good surface plasmon resonance property. In addition, a shorter lifetime means a fluorophore has less available time for photochemistry while in the excited state and hence more excitation–emission cycles before photobleaching [33].

In the present study, the enhancement mechanism may be a combination of RDE and SPCE in addition to few other effects, which will be described in detail in the following sections. In the case of fluorophores on the top of the nanocone structure, the surface plasmon will be radiated into free space, whereas in the cell imaging experiment, the surface plasmon will interact with the fluorophores inside the dielectric CHO cell that has a different refractive index.

4. Cell imaging experiment

After confirming that the substrate can provide surface plasmon coupling, we grow Chinese Hamster Ovarian (CHO) cells on the nanocone substrate. The cell membrane and DNA of the live cell are stained with fluorescent dyes in one set of experiments. In another set of experiments, fluorescent labels are applied to calcium ions in the cytoplasm and the DNA of the live cell. The labeled CHO cells on the nanocone structure are imaged using a high-resolution laser scanning confocal microscope. The 405, 488 and 561 nm spectral lines were used for the excitation of fluorophore dyes. The laser beam is illuminated on the nanocone substrate after focusing through the cell. We used an extremely low laser power and short imaging time; 0.2% of 25 mW laser power for green fluorescence excitation and 1.58 μs pixel dwell time.

4.1. Confocal imaging for fluorophore labeled to cell cytoplasm

A bright-field image of CHO cells grown on the substrate is shown in figure 3(a). For comparison purposes, we intentionally patterned the substrate surface to make an array of square areas with a silver nanocone plasmonic structure and the rest of the substrate surface is covered with a smooth silver film. The cytoplasmic calcium fluorophore emission (label in green) in the cell grown on the nanocone substrate can be observed in 3D fluorescence imaging (figure 3(b)). In contrast, the cells on a smooth silver surface express undetectable to extremely low fluorescence emission only except near the immediate surface of a smooth silver film. The fluorescence intensity below and beyond the cell span is due to the point spread function of the fluorescence emission. The vertical cross-sectional cell images (figure 3(c)) at various vertical positions show that the enhancement of the cytoplasm calcium fluorescence on the nanocone substrate extends up to the top position on the spheroidal cell, around 12 μm above the nanocone substrate. In comparison to that of the cytoplasm, the fluorescence enhancement for the nucleus fluorescence is modest. The viability of CHO cells in the imaging experiments is evident by the normal morphology expressed by the cells on the nanocone substrate after 12 h of incubation. The fluorescent expression of fluo-4 inside the cell requires cleavage of fluo-4 AM by intracellular esterase, demonstrating viable activity of enzymes in the cytoplasm and intact cell membrane [34].
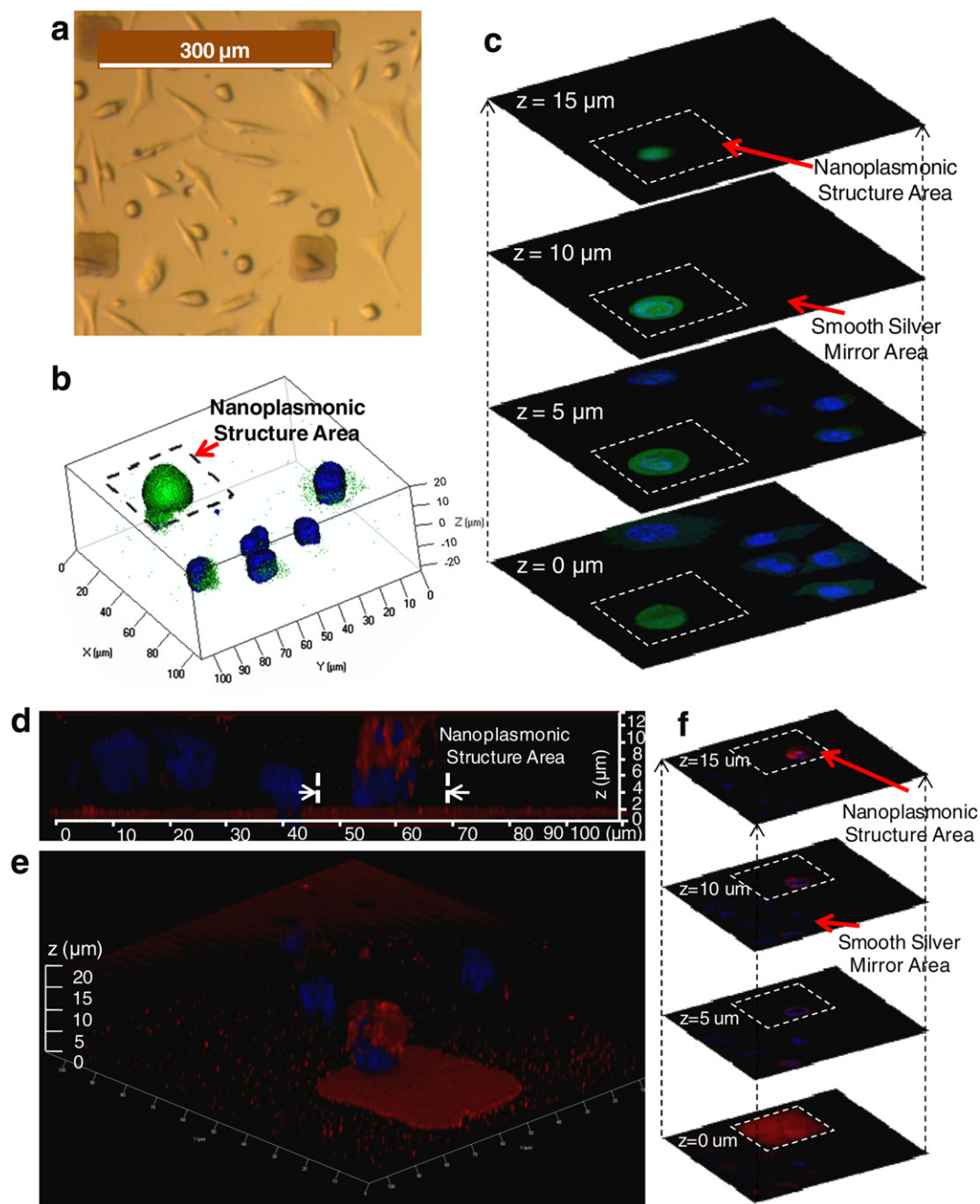
Figure 3. Confocal fluorescence microscopy imaging of live cells on the nanocone substrate. (a) Bright-field image of large number of cells grown on the substrate. (b) 3D confocal image of CHO cells on the nanocone plasmonic structure. (c) Vertical cross section of the cells at different z positions. $z = 0$ denotes the surface of the substrate and $z > 0$ is away from the surface. (d) Far-field fluorescence enhancement of the fluorophore labeled on the CHO cell membrane. (e) 3D confocal fluorescence image for the CHO cells when fluorophore is labeled on the cell membrane and nuclei of the cells. (f) Vertical cross section (z-stack) image for the cell showing the cell membrane fluorescence enhancement.

4.2. Confocal imaging for fluorophore labeled on cell membrane

To extend the generality of our interpretation, we performed another set of experiments with cell membrane and nucleus labeled by red and blue emission fluorophores, respectively. The x–z plane cross-sectional image is shown (figure 3(d)). Due to overwhelmingly high fluorescence enhancement for the 3D cell membrane on the nanocone substrate, the other cell membrane on the smooth silver surface is not visible under such a high intensity contrast. However, the fluorescence intensity of the cell nucleus on the nanocone region and that of the nuclei of the cells on the smooth silver surface are comparable. It is well known that metal-enhanced fluorescence is distance-dependent and the fluorescence is enhanced only when the fluorophore is in the vicinity of the metal nanostructure at an optimal distance of about 5–30 nm [11, 35]. The red fluorescence near the immediate
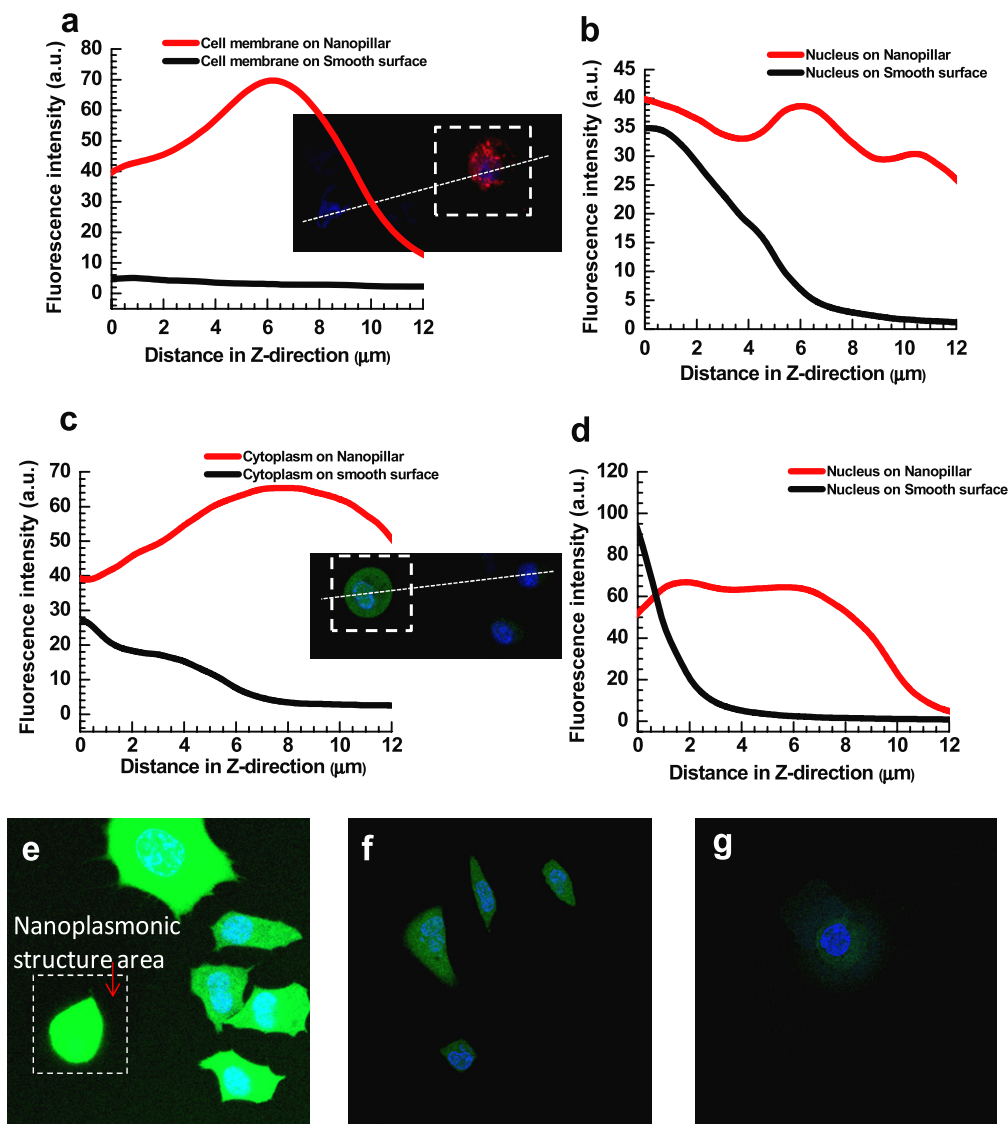
Figure 4. Quantitative analysis of fluorescence enhancement in confocal cell imaging. (a) Comparison of the average fluorescence intensity of the membrane of the cells on the silver-coated nanocone structure and on the silver-coated smooth surface. (b) Comparison of average fluorescence intensity of the nucleus of the cells on the silver-coated nanocone structure and on the silver-coated smooth metal surface. (c) Comparison of average fluorescence intensity of the fluorophore attached to the cytoplasm of the cells when it is on the silver-coated nanocone structure and on the silver-coated smooth surface. (d) Comparison of average fluorescence intensity of the nucleus of the cells on the silver-coated nanocone structure and on the silver-coated smooth surface for the case when the cytoplasm of the cell is also labeled. Confocal cell imaging with identical laser power setting (0.48 mW) and pixel dwell time (2.55 μs) for cells on a (e) silver-coated nanocone substrate, (f) smooth silicon substrate and (g) glass substrate.

surface of the substrate is due to the fluorophore staining solution out of the culture medium. However, the red fluorophore, which labels the cell membrane, is not discernible at all above the substrate surface, except for the cell sitting on the nanocone structure. The fluorescence enhancement away from the surface is further elucidated from the 3D z-stack images of the number of cells on smooth as well as nanopillar substrates (figure 3(f)). Due to overwhelming fluorescence enhancement further away from the substrate surface, the fluorescent-labeled cell membrane can be seen only for the cell on the top of the nanocone structure (figure 3(e)). The vertical cross-sectional cell images (figure 3(f)) at various z position again confirmed that the strong cell membrane fluorescence enhancement on the nanocone substrate is extending up to the

top position on the spheroidal cell, around 15 μm above the nanocone substrate.

4.3. Quantitative cell imaging analysis

The quantitative analysis for the fluorescence enhancement factor is performed by comparing the average fluorescence intensity at each depth (z coordinate) of the z-stack images taken by the confocal fluorescence microscope. The average fluorescence intensities for the cell membrane, cytoplasm and nucleus are shown in figure 4. Increasing the z distance denotes the imaging plane away from the substrate surface, that is $z = 0$ is on the substrate. The actual height or thickness of the cell is around 12 μm or $z = 12$ μm. Since the membrane of the
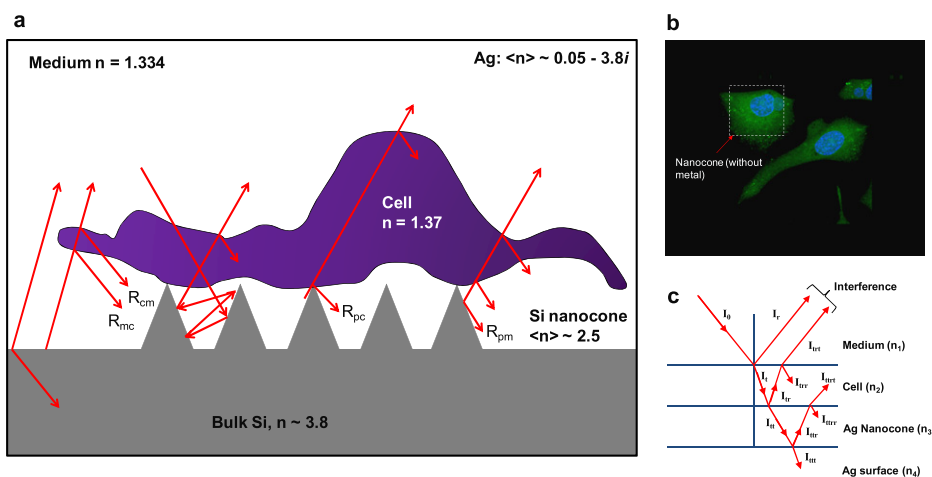
Figure 5. ((a), (c)) Multiple reflection in a nanopillar–cell system. R_{cm}: reflection at cell–medium interface; R_{mc}: reflection at medium–cell interface; R_{pc}: reflection at pillar–cell interface; R_{pm}: reflection at pillar–medium interface. (b) Confocal image of CHO cells on uncoated nanocone substrate, showing similar levels of the fluorescence intensity of the cells on the nanocone region (boxed) and on smooth region.

cells are about 7 nm thick [36], some of the fluorophores on the cell cytoskeletons that are attached to the nanocone substrate will experience the metal-enhanced fluorescence (MEF). We observed eightfold increases in fluorescence intensity of the membrane of the cell on the nanocone substrate as compared to a silver-coated smooth surface (figure 4(a)). Interestingly, this is similar to the amount of enhancement measured by fluorescence spectroscopy experiment for a red fluorescing dye R6G (figure 2(c)). The enhancement factor was calculated as [10, 12, 37]

$$\mathrm{EF} = \frac{I_M - I_{MB}}{I_G - I_{GB}}.$$

Here, I_M and I_{MB} are the fluorescence intensities of cells measured on the nanocone/flat silver surfaces and the background intensity when the cell is absent, respectively. I_G and I_{GB} are the fluorescence intensity of the cell on a glass slide and background intensity, respectively. On the cell membrane at $z = 6$ μm, we observed a 23-fold fluorescence intensity increase on the nanocone substrate compared to that on the silver-coated smooth surface. Given that the silver-coated smooth surface can provide an approximately fivefold fluorescence enhancement (figure 2(c)), the total fluorescence enhancement factor for the cell membrane obtained by the fluorescence enhancing platform will be 115-fold with respect to a glass slide surface. The calculated enhancement factor is much higher than the conventional metal-enhanced fluorescence in near-field, that is, approximately 40-fold with respect to a glass slide surface according to our spectroscopic measurement (figure 2(c)). Even by comparing the maximum fluorescence intensity measured on the silver-coated smooth surface (at $z = 0$ μm) and that on the nanocone substrate (at $z = 7$ μm), there is still a 14-fold increase on the nanocone substrate. Most interestingly, the maximum fluorescence enhancement on the silver-coated nanocone structure is found at an imaging plane far from the surface ($z = 6$–8 μm), which cannot be explained by conventional metal-enhanced fluorescence mechanisms. One of the reasons for the intensity peaking at the 6 μm position is due to the morphology of

the cell (spherical) on the nanocone substrate as compared to elongated cells on the smooth surface. As we are calculating the average integrated intensity in each plane, the mid-plane of the cell (around $z = 6$ μm) has a larger number of fluorophores and hence higher intensity as compared to the bottom of the cell. However, the overall higher intensity away from the surface of the nanocone substrate is still needed to be explained.

Similar intensity enhancement is observed for fluorophores labeled to the cell cytoplasm on the nanopillar plasmonic structure as compared to the cells on the silver-coated smooth surface (figure 4(c)). The fluorescence enhancement observed is higher for a fluorophore labeled on a cell membrane (115-fold), than when a fluorophore labeled to cytoplasm calcium (approximately 70-fold). As shown in figures 4(b) and (d), the peak fluorescence intensity for the nucleus of the cell near the smooth surface is slightly higher than that of the cell nucleus on the nanocone structure. However, the fluorescence intensity of the fluorophore labeled to the nucleus on the nanocone structure is higher than the cells on the smooth surface further away from the substrate plane. To illustrate our point more clearly, cells on two control samples (glass and smooth silicon substrate) and nanocone structure are imaged using the same imaging parameters' set-up (laser power of 0.48 mW, pixel dwell time of 2.55 μs). As shown in figures 4(e)–(g) the higher fluorescence intensity for the cells on the nanocone structure can be clearly seen. In fact, with this higher power and long integration time setting the cell image intensity on the nanocone structure becomes saturated due to the extremely high enhancement. In order to exclude the possibility of cell fluorescence increase due to mechanical stimulation of the nanocone structure, we carry out confocal imaging of CHO cells on a silicon nanocone control sample without any silver coating. Figure 5(b) shows both the fluorophore channels: fluorophore labeled to the cytoplasm of the cell and fluorophore labeled to the nucleus of the cell. Clearly, the fluorescence intensity of the cells on an uncoated nanocone substrate and on an uncoated smooth surface is quite similar.

We believe light trapping is taking place inside the cell. In a device (cell) 'light trapping' will happen if the optical path length is several times the actual device (cell) thickness. Here the optical path length of a device is defined as the distance that an unabsorbed photon may travel within the device before it escapes out of the device. Light trapping is usually achieved by changing the angle at which light travels in the cell, making the light enter the cell at critical angles. A textured surface will not only reduce reflection as previously described but will also couple light obliquely into the cell, thus giving a longer optical path length. Due to multiple random reflections, light can be trapped inside the cell and will make multiple passes through the cell, thus allowing higher fluorescence intensity. Local variations in refractive index are the basic physical cause for light scattering in optical media. The average refractive index of living cells depends mostly on the protein concentration. A typical mammalian cell has an average protein content of 18% mass [38], corresponding to a refractive index of about 1.37. The main components of cell membranes are phospholipids, cholesterol and membrane-spanning proteins and usually have a higher refractive index than the proteins in the cytoplasm. The refractive index of membranes is about 1.48 [39]. This difference in refractive index between cytoplasm and membranes will have an impact on the light scattering properties inside the cells. Differences in refractive index influence the phase of the propagating light waves [40]. As shown in figures 5(a) and (c), part of incident light (I_0) is reflected (I_r) and the remainder is refracted/transmitted (I_t) at the interface. As the transmitted light (I_t) encounters another interface, it will undergo partial reflection (I_{tr}) and partial transmission (I_{tt}) and so on. Since these light waves are components of the same wave, they will have the same frequency, but can have different phases [41]. Constructive interference of the reflected light wave can give rise to higher intensity. But how does the light enter the cell? The evanescent electric field is generated at the optical frequency due to a propagating surface plasmon at the tip of the nanocone. The evanescent field penetrates the cell with an exponentially decaying intensity, that falls by a factor, $1/e$, just 100 nm from the interface [42]. This light undergoes multiple reflections inside the cell due to the differences in refractive index inside the cell. The cell membrane has a higher refractive index than the outside buffer solution. There is also a possibility of total internal reflection inside the cell when light is traveling from a high to a low refractive index medium. For example, with membrane RI of 1.48 and PBS buffer RI of 1.334 [43], the critical angle for total internal reflection to occur is 64.3363°. Hence we argue that strong scattering occurs within a nanostructured area (shown by a strong SERS signal), and due to random reflection inside the cell resulting in the observed enhancement in fluorescence further away from the substrate surface.

5. Conclusions

The nanoplasmon surface composed of nanocone structures is a platform for three-dimensional fluorescence enhanced cell imaging with high sensitivity. We have demonstrated that the nanoplasmon surface can enhance the fluorescence signal from a cell membrane (FM 1-43 FX) by 115-fold and from a cell cytoplasm (Fluo-4, AM) by 70-fold. We anticipate that the nanocone surface can provide higher intensity for the dyes labeled to the cells and at the same time less photobleaching on the dyes and hence will be an ideal candidate as a microscopy substrate to observe very early stage protein expressions after transfection.

References

[1] Lichtman J W and Conchello J A 2005 Fluorescence microscopy *Nature Methods* **2** 910–9

[2] Inoue S and Oldenbourg R 1995 Microscopes *Handbook of Optics* 2nd edn (New York: McGraw-Hill)

[3] Le Moal E *et al* 2007 Mirror slides for high-sensitivity cell and tissue fluorescence imaging *J. Biomed. Opt.* **12** 024030

[4] Le Moal E, Lévêque-Fort S, Fort E, Lacharme J P, Fontaine-Aupart M P and Ricolleau C 2005 Active substrates improving sensitivity in biomedical fluorescence microscopy *Proc. SPIE* **5860** ThF1

[5] Le Moal E, Fort E, Leveque-Fort S, Cordelieres F P, Fontaine-Aupart M and Ricolleau C 2007 Enhanced fluorescence cell imaging with metal-coated slides *Biophys. J.* **92** 2150–61

[6] Moskovits M 1985 Surface-enhanced spectroscopy *Rev. Mod. Phys.* **57** 783–826

[7] Geddes C D and Lakowicz J R 2002 Metal-enhanced fluorescence *J. Fluoresc.* **12** 121–9

[8] Aslan K, Gryczynski I, Malicka J, Matveeva E, Lakowicz J R and Geddes C D 2005 Metal-enhanced fluorescence: an emerging tool in biotechnology *Curr. Opin. Biotechnol.* **16** 55–62

[9] Pompa P P *et al* 2006 Metal-enhanced fluorescence of colloidal nanocrystals with nanoscale control *Nature Nanotechnol.* **1** 126–30

[10] Cui X, Tawa K, Kintaka K and Nishii J 2010 Enhanced fluorescence microscopic imaging by plasmonic nanostructures: from a 1D grating to a 2D nanohole array *Adv. Funct. Mater.* **20** 945–50

[11] Lee K, Hahn L D, Yuen W W, Vlamakis H, Kolter R and
     Mooney D J 2011 Metal-enhanced fluorescence to quantify
     bacterial adhesion *Adv. Mater.* **23** 101

[12] Cui X, Tawa K, Hori H and Nishii J 2010 Tailored plasmonic
     gratings for enhanced fluorescence detection and
     microscopic imaging *Adv. Funct. Mater.* **20** 546–53

[13] Lakowicz J R 2005 Radiative decay engineering 5:
     metal-enhanced fluorescence and plasmon emission *Anal.
     Biochem.* **337** 171–94

[14] Balaa K and Fort E 2009 Nikon instruments. Surface plasmon
     enhanced TIRF imaging *Imaging Microsc.* **11** 55–6

[15] Willets K A and Van Duyne R P 2007 Localized surface
     plasmon resonance spectroscopy and sensing *Annu. Rev.
     Phys. Chem.* **58** 267–97

[16] Knoll W 1998 Interfaces and thin films as seen by bound
     electromagnetic waves *Annu. Rev. Phys. Chem.* **49** 569–638

[17] Raether H Surface-plasmons on smooth and rough surfaces and
     on gratings 1988 Springer *Tracts Mod. Phys.* **111** 1–133

[18] Popov E, Bonod N and Enoch S 2007 Comparison of plasmon
     surface waves on shallow and deep metallic 1D and 2D
     gratings *Opt. Exp.* **15** 4224–37

[19] Gartia M R *et al* 2010 Rigorous surface enhanced Raman
     spectral characterization of large-area high-uniformity
     silver-coated tapered silica nanopillar arrays
     Nanotechnology **21** 395701

[20] Arya K, Su Z B and Birman J L 1985 Localization of the
     surface plasmon polariton caused by random roughness and
     its role in surface-enhanced optical phenomena *Phys. Rev.
     Lett.* **54** 1559

[21] Stockman M I 2004 Nanofocusing of optical energy in tapered
     plasmonic waveguides *Phys. Rev. Lett.* **93** 137404

[22] Ghaemi H F, Thio T, Grupp D E, Ebbesen T W and Lezec H J
     1998 Surface plasmons enhance optical transmission
     through subwavelength holes *Phys. Rev.* B **58** 6779–82

[23] Chaturvedi P, Hsu K H, Kumar A, Fung K H, Mabon J C and
     Fang N X 2009 Imaging of plasmonic modes of silver
     nanoparticles using high-resolution cathodoluminescence
     spectroscopy *ACS Nano* **3** 2965–74

[24] de Abajo F J G and Kociak M 2008 Probing the photonic local
     density of states with electron energy loss spectroscopy
     Phys. Rev. Lett. **100** 106804

[25] Gerber S, Reil F, Hohenester U, Schlagenhaufen T, Krenn J R
     and Leitner A 2007 Tailoring light emission properties of
     fluorophores by coupling to resonance-tuned metallic
     nanostructures *Phys. Rev.* B **75** 073404

[26] Farcau C and Astilean S 2009 Silver half-shell arrays with
     controlled plasmonic response for fluorescence enhancement
     optimization *Appl. Phys. Lett.* **95** 193110

[27] Qiu T, Jiang J, Zhang W, Lang X, Yu X and Chu P K 2010
     High-sensitivity and stable cellular fluorescence imaging by
     patterned silver nanocap arrays *ACS Appl. Mater. Interface*
     2 2465–70

[28] Geddes C D, Gryczynski I, Malicka J, Gryczynski Z and
     Lakowicz J R 2004 Fluorescence detection gains in
     sensitivity *Photon. Spectra* **38** 92

[29] Isfort G, Schierbaum K and Zerulla D 2006 Causality of
     surface plasmon polariton emission processes *Phys. Rev.* B
     73 033408

[30] Zhang Y, Aslan K, Previte M J R and Geddes C D 2007
     Metal-enhanced fluorescence: surface plasmons can radiate
     a fluorophore's structured emission *Appl. Phys. Lett.*
     90 053107

[31] Shibamoto K, Katayama K, Fujinami M and Sawada T 2003
     Fundamental processes of surface enhanced Raman
     scattering detected with transient reflecting grating
     spectroscopy *Rev. Sci. Instrum.* **74** 910–2

[32] Zhang J, Matveeva E, Gryczynski I, Leonenko Z and
     Lakowicz J R 2005 Metal-enhanced fluoroimmunoassay on
     a silver film by vapor deposition *J. Phys. Chem.* B
     109 7969–75

[33] Zhang J, Fu Y, Chowdhury M H and Lakowicz J R 2008
     Plasmon-coupled fluorescence probes: effect of emission
     wavelength on fluorophore-labeled silver particles *J. Phys.
     Chem.* C **112** 9172–80

[34] Gee K R, Brown K A, Chen W N, Bishop-Stewart J,
     Gray D and Johnson I 2000 Chemical and physiological
     characterization of fluo-4 Ca(2+)-indicator dyes *Cell
     Calcium* **27** 97–106

[35] Mertens H, Koenderink A F and Polman A 2007
     Plasmon-enhanced luminescence near noble-metal
     nanospheres: comparison of exact theory and an improved
     Gersten and Nitzan model *Phys. Rev.* B **76** 115123

[36] Alberts B, Johnson A, Lewis J, Raff M, Roberts K and
     Walter P 2007 *Molecular biology of the Cell* 5th edn
     (New York: Garland Science)

[37] Guo S, Heetderks J J, Kan H and Phaneuf R J 2008 Enhanced
     fluorescence and near-field intensity for Ag
     nanowire/nanocolumn arrays: evidence for the role of
     surface plasmon standing waves *Opt. Exp.* **16** 18417–25

[38] Alberts B, Bray D, Lewis J, Raff M, Roberts K and Watson J D
     1994 *Macromolecules: Structure, Shape, and Information.
     Molecular Biology of the Cell* (New York: Garland Science)
     pp 89–138

[39] Beuthan J, Minet O, Helfmann J, Herrig M and Muller G 1996
     The spatial variation of the refractive index in biological
     cells *Phys. Med. Biol.* **41** 369–82

[40] Michael R, van Marle J, Vrensen G F J M and
     van den Berg T J T P 2003 Changes in the refractive index of
     lens fibre membranes during maturation-impact on lens
     transparency *Exp. Eye Res.* **77** 93–9

[41] Cornelese-ten Velde I, Bonnet J, Tanke H J and Ploem J S 1988
     Reflection contrast microscopy: visualization of
     (peroxidase-generated) diaminobenzidine polymer products
     and its underlying optical phenomena *Histochemistry*
     89 141–50

[42] Mashanov G I, Tacon D, Knight A E, Peckham M and
     Molloy J E 2003 Visualizing single molecules inside living
     cells using total internal reflection fluorescence microscopy
     Methods **29** 142–52

[43] Chien F C and Chen S J 2006 Direct determination of the
     refractive index and thickness of a biolayer based on coupled
     waveguide-surface plasmon resonance mode *Opt. Lett.*
     31 187–9